

Non-statistical decay and α -correlations in the $^{12}\text{C}+^{12}\text{C}$ fusion-evaporation reaction at 95 MeV

L Morelli¹, G Baiocco^{1,2} ‡, M D’Agostino¹, F Gulminelli²,
M Bruno¹, U Abbondanno³, S Appannababu⁴, S Barlini^{5,6},
M Bini^{5,6}, G Casini⁶, M Cinausero⁴, M Degerlier⁷,
D Fabris⁸, N Gelli⁶, F Gramegna⁴, V L Kravchuk^{4,9},
T Marchi⁴, A Olmi⁶, G Pasquali^{5,6}, S Piantelli⁶, S Valdré^{5,6}
and Ad R Raduta¹⁰

¹Dipartimento di Fisica ed Astronomia dell’Università and INFN, Bologna, Italy

²LPC (IN2P3-CNRS/Ensicaen et Université), F-14076 Caen cédex, France

³INFN Trieste, Italy

⁴INFN, Laboratori Nazionali di Legnaro, Italy

⁵Dipartimento di Fisica ed Astronomia dell’Università, Firenze, Italy

⁶INFN Firenze, Italy

⁷ University of Nevsehir, Science and Art Faculty, Physics Department, Nevsehir, Turkey

⁸INFN, Padova, Italy

⁹National Research Center “Kurchatov Institute”, Moscow, Russia

¹⁰NIPNE, Bucharest-Magurele, POB-MG6, Romania

E-mail: luca.morelli@bo.infn.it

Abstract. Multiple alpha coincidences and correlations are studied in the reaction $^{12}\text{C}+^{12}\text{C}$ at 95 MeV for fusion-evaporation events completely detected in charge. Two specific channels with Carbon and Oxygen residues in coincidence with α -particles are addressed, which are associated with anomalously high branching ratios with respect to the predictions by Hauser-Feshbach calculations. Triple alpha emission appears kinematically compatible with a sequential emission from a highly excited Mg. The phase space distribution of $\alpha-\alpha$ coincidences suggests a correlated emission from a Mg compound, leaving an Oxygen residue excited above the threshold for neutron decay. These observations indicate a preferential α emission of ^{24}Mg at excitation energies well above the threshold for $6-\alpha$ decay.

PACS numbers: 25.70.z, 24.60.Dr, 27.30.+t, 24.10.Pa

NUCLEAR REACTIONS $^{12}\text{C}(^{12}\text{C},X)$, $E = 95$ A MeV, Measured Fusion-evaporation reactions, Observed deviation from statistical behaviour. Studied fragment-particle correlation observables.

1. Introduction

Since the first heuristic proposition of α -chains as possible building blocks of even-even nuclei in the late sixties [1], the subject of α -clustering has been a central issue in nuclear physics. It has even witnessed a gain of interest in recent years [2]. On the theoretical side, highly sophisticated ab-initio calculations have shown pronounced cluster features in the ground state of a large number of light nuclei [3]. In addition, in recent years, different constrained density functional approaches have consistently found clear α -cluster correlations in all light and medium-heavy even-even nuclei at excitation energies around the threshold of breakup into constituent clusters [4, 5, 6, 7]. Concerning experimental research, rotational bands consistent with α -cluster structures have been identified in different even-even light nuclei and shown to persist even along their isotopic chains [2]. Exotic non-statistical decays of these correlated states have been evidenced in the recent literature [8].

A natural extension of the concept of nuclear clusters concerns nuclear molecules. Molecular states have been sought for in nuclear reactions since the early days of heavy-ion science. In particular, several interesting resonances have been observed in the $^{12}\text{C}+^{12}\text{C}$ reaction in the inelastic [9] and α -transfer channels [10]. These studies suggest that resonant structures persist in the ^{24}Mg system up to around 50 MeV excitation energy. This is a surprising result as a pure statistical behaviour might be expected due to the extremely high number of available states at such high excitation. Concerning the α -transfer channel, experimental results have been reproduced by coupled cluster calculations [11] where the cross section is dominated by a four-cluster $(\alpha + \alpha) + (\alpha + ^{12}\text{C})$ state of highly excited ^{24}Mg around 30 MeV. Because of the remarkable persistence of cluster correlations at high excitation energies, the question naturally arises whether such correlations might affect other dissipative channels. These are typically associated with the formation of a compound nucleus, that is a system whose decay is assumed to be fully decoupled from the reaction entrance channel and governed by purely statistical laws.

In a recent paper [12] we have analyzed $^{12}\text{C}+^{12}\text{C}$ dissipative reactions at 95 MeV and compared the experimental data to the results of a dedicated Monte Carlo Hauser-Feshbach code [13] (HF ℓ from now on) for the evaporation of the CN ^{24}Mg , at $E^*/A = 2.6$ MeV, issued in case of complete fusion. The angular momentum input distribution for the fused system in this reaction is assumed to be a triangular one, with a maximum value $J_{0\text{ max}} = 12 \hbar$, coming from the systematics [14]. Because of parity conservation, only even values of J_0 extracted from the triangular distribution are allowed as an input for the CN angular momentum.

We have shown that all the observables of dissipative events are fully compatible with a standard statistical behaviour, with the exception of α -yields in coincidence with Oxygen residues.

Specifically, the experimental Oxygen channel is dominated by the presence of two α particles in coincidence, while the Hauser-Feshbach theory predicts that the evaporation

chains leading to an Oxygen residue preferentially consist of one α and two Hydrogen isotopes. A new data measurement of the same reaction has allowed us to analyze these deviations in further details, and the results are reported in the first paper [15] of this series, hereby called paper I. The new data set has confirmed the previous results, and additionally shown an anomalously high branching ratio associated with the C - 3α channel. A cleaner event selection and a more refined analysis led to an improved data reproduction by our theoretical calculations. In the present work, which is a continuation of paper I, we analyse the kinematical correlations in these specific channels to gather further information on the emission mechanism.

The paper is organized as follows. The observed deviations from a standard statistical behaviour are summarized in §2. In the same section we show that such deviations cannot be attributed to a memory of the entrance channel. §3 deals with the multiple α correlations in non-statistical channels. Conclusions are drawn in §4.

2. Deviations from a statistical behaviour

As explained in greater details in paper I, we have measured the $^{12}\text{C}+^{12}\text{C}$ reaction at 95 MeV with the GARFIELD+RCO set-up [16]. We have selected a data-set consisting of events completely detected in charge ($Z_{tot} = 12$) which corresponds to a large extent to the complete fusion-evaporation channel. The statistical character of the data set is demonstrated by the good reproduction of a very large set of inclusive and exclusive observables by HF ℓ calculations.

Further details can be found in paper I, where we have shown that the stringent condition $Z_{tot} = 12$ does not artificially bias the global event shape: the quality of the statistical model reproduction of the different inclusive observables is the same with $Z_{tot} \geq 10$ or $Z_{tot} = 12$. However, an anomaly is observed in the probability of multiple α emission, as we show in the following.

Figure 1 summarizes the static observables related to α production. First results were already shown in [12, 15].

2.1. Multiple α coincident yields

From the inclusive charge distribution displayed in the left part of Figure 1 we can see that the statistical model well reproduces the global shape of the charge distribution, including the α production. However, as shown in the right part of Figure 1, it fails to reproduce the coincident yield (M_α). Specifically, it underestimates the number of events with $M_\alpha > 1$, while it overestimates those where no alphas are emitted. The underestimation of 4 and 5 α 's channels is clearly linked to the missing yield of the lightest residues that we can see in the left part of the figure. We have already discussed this feature in paper I and tentatively attributed it to the lack of the fragment break-up channel in the statistical model, channel which is expected to be open at these high excitation energies (2.6 AMeV).

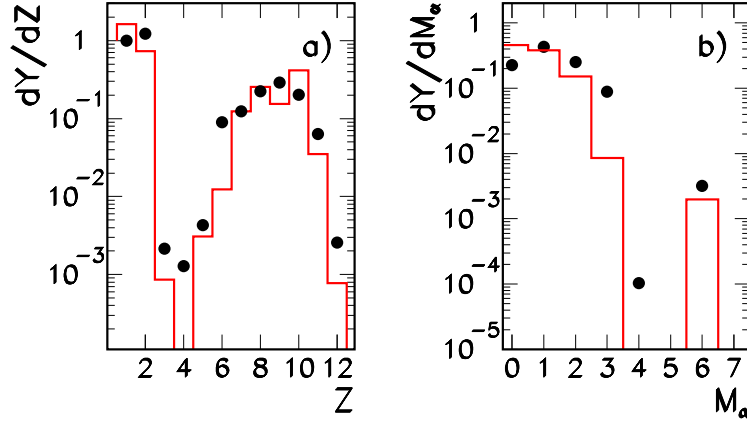


Figure 1. (Color online) Left part: Inclusive charge distribution of events completely detected in charge. For the same data set, the right part displays the α -particle multiplicity distribution. Experimental data (symbols) are compared to filtered HFℓ calculations (lines). All distributions are normalized to the total number of events.

At first sight, the presence of a peak in the multiplicity distribution corresponding to the complete decomposition of the system in constituent α -particles ($M_\alpha = 6$) could evoke a vaporized phase [18, 19] or a signature of Bose-Einstein condensation [20]. However, the presence of such a peak is predicted by a standard evaporation chain from an even-even compound, due to the large branching ratio towards α decay at each step of the de-excitation chain. This shows that the presence of a peak of multiple- α coincidences is not a sufficient evidence of α clustering, even if this possibility cannot be excluded. For this reason, we will study the kinematical properties of these events in greater detail in §3.3.

Another important effect observed in the inclusive charge distribution is related to the strong underestimation of the Carbon production yield. This could be due to a low predicted value for the α decay probability of the parent nuclei (Ne, O, Mg), or alternatively to the presence of direct reactions in the experimental sample. This reduced Carbon yield can be associated with the underestimation of triple α coincidences observed in the right part of the figure, where there is no gate on the residue charge.

Moreover, looking at Figure 2, which displays the average α yield associated with each residue \S , it can be noticed that the α multiplicity associated with Carbon residues is clearly higher in the data. This difference was already shown in [15], where we have observed that the measured branching ratio of the channel $C+3\alpha$ significantly overrates the predicted value. Figure 2 shows another significant difference of branching

\S No theoretical point is associated with $Z=3$ and 4 because HFℓ does not produce a $Z=3,4$ as the

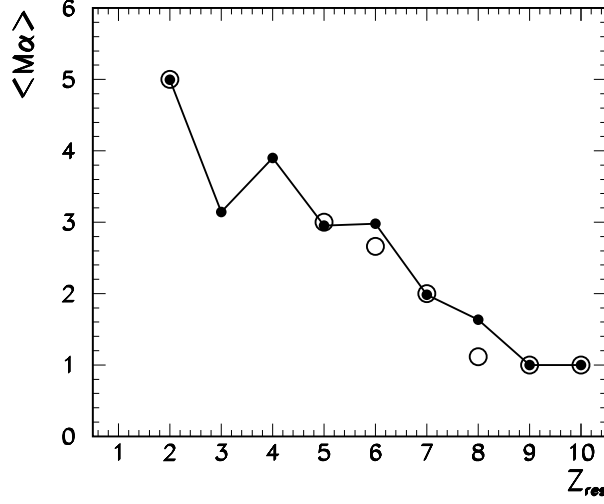


Figure 2. Experimental (full circles) and predicted (open circles) average α -particle multiplicity as a function of the charge of the heaviest fragment. Events where no α -particles are emitted are excluded in this analysis.

ratios between model and data concerning the Oxygen channel: the α multiplicity in coincidence with Oxygen again overcomes the statistical predictions. Similarly to the Carbon case, the dominant charge channel populated by $\text{HF}\ell$ in coincidence with Oxygen is $(2H - \alpha - O)$, in contradiction with the experimental measurement (see paper I). It is interesting to remark that this deviation is washed out in the multiplicity distribution in Figure 1, because of the large number of channels implying two coincident α -particles.

To put in a better evidence possible α clustering effects, we can define a variable quantifying the experimental branching ratio excess for α emission:

$$R_{clus}(Z) = \frac{Y_{exp}(Z; n_Z \alpha)}{Y_{exp}(Z)} - \frac{Y_{HF\ell}(Z; n_Z \alpha)}{Y_{HF\ell}(Z)} \quad (1)$$

Here $Y(Z; n_Z \alpha)$ ($Y(Z)$) indicate coincident (inclusive) yields; $n_Z \alpha$ is the (nearest integer) maximum α multiplicity associated with the residue of charge Z ($n_Z \alpha = (12 - Z)/2$). The subscripts “exp” and “ $\text{HF}\ell$ ” refer to experimental data and model predictions, respectively.

The extra probability of α emission defined by (1) is plotted in Figure 3. We can see that, in agreement with Figure 2, the evaporation chains leading to a final Carbon or Oxygen residue show a preferential α decay. A smaller effect in the same direction is visible for a Neon residue.

A possible interpretation of this α excess may be due to the presence of residual α structure correlations in the excited ^{24}Mg or in its daughter nucleus ^{20}Ne . We must notice that the excitation energy of the compound $E^*(^{24}\text{Mg}) = 62.4$ MeV is well above

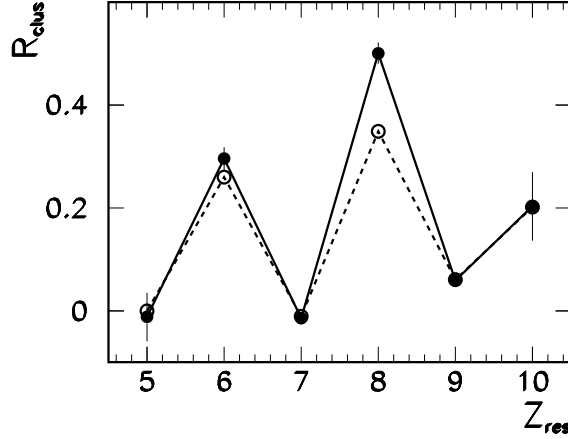


Figure 3. Branching ratio excess for α decay as a function of the atomic number of the final residue. Full symbols: all events. Open symbols: more dissipative events only. Lines are drawn to guide the eye. All distributions are normalized to the unitary area.

the threshold for multiple- α decay, where such correlations are expected. However the average α energy in the center of mass results to be 10.5 MeV and according to the HF ℓ calculation this energy is increased to 13 MeV for the first chance emission. After the first evaporation step, considering the Q-value of the decay, the daughter nucleus is expected to be at an excitation energy $E^*(^{20}\text{Ne}) \approx 40$ MeV. This value is still much higher than the energy threshold for 5- α dissociation $E_{theo}^*(^{20}\text{Ne}) \approx 16.74$ MeV where cluster states are theoretically expected [5, 7], but cluster structures at energies as high as 30 MeV have been already reported in the literature [11].

To explore the possibility of alpha structure correlations in the continuum, we now turn to study α -channels in greater detail.

2.2. The influence of dissipation

The well-known peculiarity of the $^{12}\text{C}+^{12}\text{C}$ fusion-evaporation reaction is that both the entrance channel and the compound nucleus have potentially α structure correlations. In particular, inelastic and α transfer reactions could be mixed to fusion-evaporation events, thus explaining the failure of the statistical model to correctly reproduce the Carbon and Oxygen channel. The distinction between direct and compound reactions is not completely well defined. Indeed the physical processes are continuous and the compound ^{24}Mg could be in a quasi-molecular state reminiscent of the entrance channel, even if it is the source of α emission. A clear distinction between entrance channel effects and compound effects can only be done by comparing the decay of the ^{24}Mg

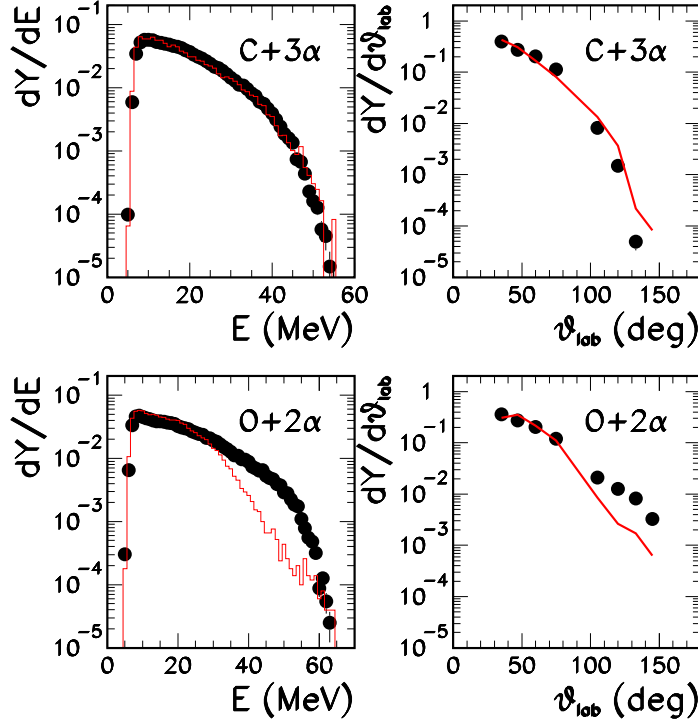


Figure 4. (Color online) Energy spectra (left) and angular distributions (right) of α -particles detected in coincidence with a Carbon (upper part) or an Oxygen (lower part) residue. Data (symbols) are compared to HF ℓ calculations (lines). All distributions are normalized to the unitary area.

formed in two different entrance channels leading to the same excitation energy. To this aim, we have measured the reaction $^{14}\text{N}+^{10}\text{B}$ at 80.7 MeV. Although the data are still under evaluation, preliminary results [17] show indeed a reduction of the ($^4\text{O}-2\alpha$) channel in this second reaction with respect to the $^{12}\text{C}+^{12}\text{C}$ one. A complete study is in preparation.

Direct reactions typically lead to angular distributions which are reminiscent of the entrance channel and therefore forward-backward peaked in the laboratory system. This can be a hint to at least partially disentangle the two mechanisms within a single dataset. An indication in this sense comes from inspection of Figure 4. This figure shows the energy spectrum and angular distribution of α -particles emitted in coincidence either with a Carbon or with an Oxygen residue, in comparison with the HF ℓ calculation. While the Carbon channel does not show any indication of memory of the entrance channel, a clear deviation is seen with respect to the statistical model in the Oxygen case. Specifically, an excess of backward emitted α -particles (corresponding to low energy in the laboratory frame) could indicate an incomplete memory loss of the entrance channel

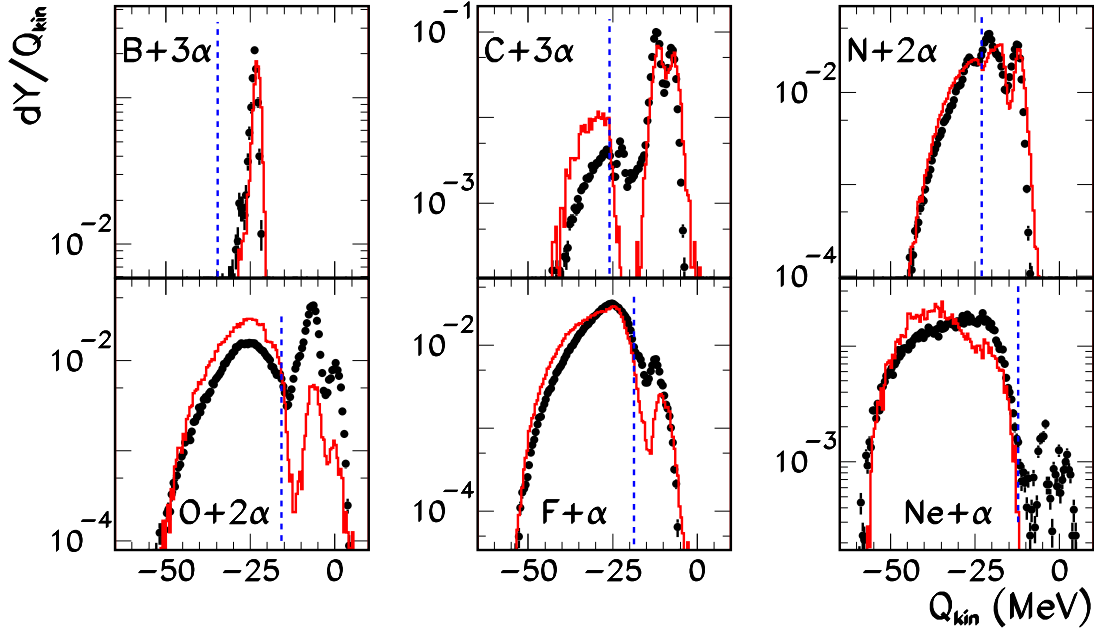


Figure 5. (Color online) Q_{kin} distributions in complete events ($Z_{tot} = 12$) where the residue of charge from 5 to 10, indicated in each panel, is detected in coincidence with the maximum possible number of α -particles. Data (symbols) are compared to HF ℓ calculations (red lines). The dashed lines indicate the threshold Q -value for neutron emission that we have adopted to separate more dissipative from less dissipative events. All distributions are normalized to unitary area.

and a contamination from direct reactions in our experimental sample.

To further explore this hypothesis, we study the α -channels as a function of the dissipated energy. We introduce an estimate of the dissipation by the event-by-event quantity:

$$Q_{kin} = E_{kin} - E_{beam} = \sum_{i=1}^N E_i - E_{beam} \quad (2)$$

where E_i is the energy of the particle in the laboratory frame and the sum extends to the N particles or fragments that are detected in coincidence, and exhausts the total charge $Z_{tot} = 12$. The quantity Q_{kin} corresponds to the real Q -value of the reaction, given by the mass balance between the initial and final state, provided that the whole mass is collected in the outgoing channel (that is, in the absence of neutron emission).

Figure 5 displays the experimental (symbols) and theoretical (lines) Q_{kin} distributions for the channels corresponding to the maximum α multiplicity associated with the residue of charge Z .

We can see that the theoretical and experimental spectra show a common structure, with narrow peaks at high Q_{kin} values, and a broader region extending up to an important amount of missing energy. In the model calculations, the different peaks correspond to the various evaporation chains, starting from the $^{24}\text{Mg}^*$ compound nucleus, and finally leaving a residue of charge Z in one of its isotopic ground or low lying excited states. Despite the limited energy resolution in the Q_{kin} reconstruction, which broadens the peaks, the different levels can be clearly recognized in the experimental sample and correspond to the predicted ones.

Starting from the threshold value of neutron emission associated with each residue (dashed line in Figure 5), a continuous contribution due to the missing neutron energy is superimposed to the discrete Q_{kin} spectrum. This contribution becomes dominant in more dissipative events associated with low Q_{kin} values, where neutron emission from the continuum is the dominant decay mechanism. We will call from now on, as in [15], $Q_{<}$ and $Q_{>}$ the two regions below and above the neutron emission threshold, respectively.

Besides the common pattern observed for the theoretical and experimental Q_{kin} distributions, clear differences are evident in the relative population of the different regions, between experimental data and calculations in Figure 5. The larger deviations correspond to even- Z residues. As in the case of the previous observables, this could be due to an underestimation by the model of the α decay probability of even- Z nuclei or due to the presence of direct reactions in the experimental sample.

In particular, for the Neon residue, the model does not produce events in the $Q_{>}$ region. This deviation of the data from a statistical behaviour could be attributed to inelastic reactions due to quasi-molecular states of the compound ^{24}Mg , reminiscent of the entrance channel. The comparison with another reaction [17], where the same compound nucleus is formed by non α -like reaction partners could shed some light on these discrepancies.

In the present paper we limit ourselves to the Oxygen and Carbon residues, i.e. to (2α - ^4O) and (3α - ^4C) coincidences. The highest Q_{kin} peak ($Q_{kin} \approx 0 \text{ MeV}$ for O , $Q_{kin} \approx -7.3$ for C) corresponds to the respective ground state of ^{16}O and ^{12}C . In the statistical calculation these peaks are obtained when the last-step α emission from the $^{24}\text{Mg}^*$ compound nucleus leaves the residue directly in its ground state. The lower Q_{kin} peaks ($Q_{kin} \approx -6.5 \text{ MeV}$ for O , $Q_{kin} \approx -11.7$ for C) correspond to the population of one of the particle bound excited states of ^{16}O and ^{12}C , which further γ -decay to the respective ground state.

Starting from the threshold value for neutron emission ($Q_{kin} = -15.8 \text{ MeV}$ for ^{15}O , $Q_{kin} = -26.0$ for ^{11}C) a broader distribution is observed due to neutron emission, and the amount of missing energy corresponds to the undetected neutron kinetic energy.

Specifically, in the 2α - ^4O channel a much higher percentage of events populates the $Q_{>}$ region in the experimental sample with respect to model predictions. The larger experimental branching ratio for the multiple α exit channel in the $Q_{>}$ region is another indication of a possible contamination from direct reactions involving an excited ^{12}C nucleus, in competition with fusion evaporation.

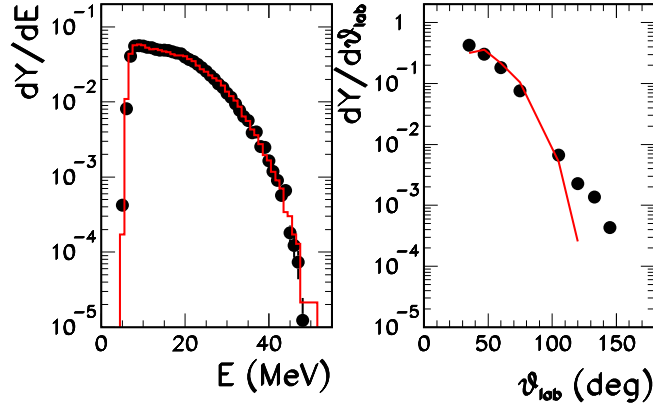


Figure 6. (Color online) Energy spectra (left) and angular distributions (right) of α -particles detected in coincidence with an Oxygen residue in the 2α - ^AO events, for the most dissipative region $Q_{<}$ (see text). Data (symbols) are compared to HF ℓ calculations (lines). All distributions are normalized to the unitary area.

Figure 6 presents the α energy spectrum and the angular distribution obtained when the less dissipative ($Q_{>}$) events are excluded from the analysis. We can see that the agreement between data and model is improved, confirming the direct nature of the less dissipative $Q_{>}$ events.

On the contrary in the 3α - ^AC channel the Q_{kin} distribution is quite well reproduced by the model. A slightly different proportion of more dissipative $Q_{<}$ versus less dissipative $Q_{>}$ can be observed between the two samples, but the main discrepancy concerns the small peak between $Q_{kin} = -20$ and -24 MeV, which is observed in the experimental Carbon spectrum, and it is not visible in the calculation (see Figure 5 middle upper panel).

In agreement with previous evaluations [12], this peak corresponds to a contribution of about 3% from the channel $^{13}\text{C}+^3\text{He}+2\alpha$ ($Q_{kin} = -22.9$ MeV). This $^3\text{He}-\alpha$ contamination is due to $Z = 2$ particles at the limit of the mass identification threshold.

If we limit our attention to the true 3α - ^AC coincidences, we can conclude that the overall shape of the Q_{kin} spectrum is consistent with a statistical behaviour. The main significant deviation associated with Carbon is the overall higher experimental probability of the 3α - ^AC channel, independently of the dissipation (see Figure 2 and paper I).

This discrepancy in the C channel may be due to a preferential α -particle emission by the reaction partners, followed by a standard compound nucleus decay of the incomplete fused source. To investigate this hypothesis, we show in Figure 7 the correlation between the laboratory parallel velocities of the detected C residue and

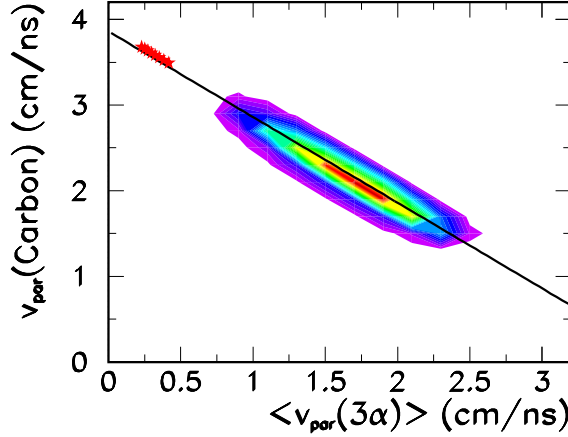


Figure 7. (Color online) Logarithmic contour plot of the correlation between the laboratory parallel velocity of the detected C residue and the laboratory parallel velocity of the center of mass of the three α -particles for all Q_{kin} values. The solid line is the expected correlation from the parallel momentum conservation in the laboratory system. The stars give the kinematical locus of binary reactions compatible with the detection of a quasi-projectile Carbon fragment in the experimental apparatus.

The correlation of Figure 7 shows a single peak close to the center of mass velocity (≈ 2 cm/ns in this experiment). The kinematical locus associated with alpha emission in a pure dissipative two-body kinematics is indicated by the stars in the figure. Contribution of peripheral binary reactions is therefore excluded. The experimental distribution can rather suggest the decay from quasi-molecular states of the excited ^{24}Mg .

Summarizing, only in the case of Oxygen a contamination from direct reactions can contribute to the discrepancy between the data and the statistical model. However, excluding the $Q_{>}$ less dissipative events in the Oxygen channel, a large branching ratio discrepancy is still observed. This is shown by the dashed line in Figure 3, where the clusterization excess defined by (1) is evaluated only for more dissipative events. Even in this case, an important branching ratio excess for multiple α emission is observed with respect to the statistical model. It is therefore clear that another mechanism is at play in these channels and specific excited states with pronounced cluster structures are populated.

In the next section we turn to study the kinematical properties of the multiple α channels to better understand the reaction mechanism or emission sequence leading to such events.

3. Multiple α correlations

3.1. $^A\text{O}-\alpha-\alpha$ correlations

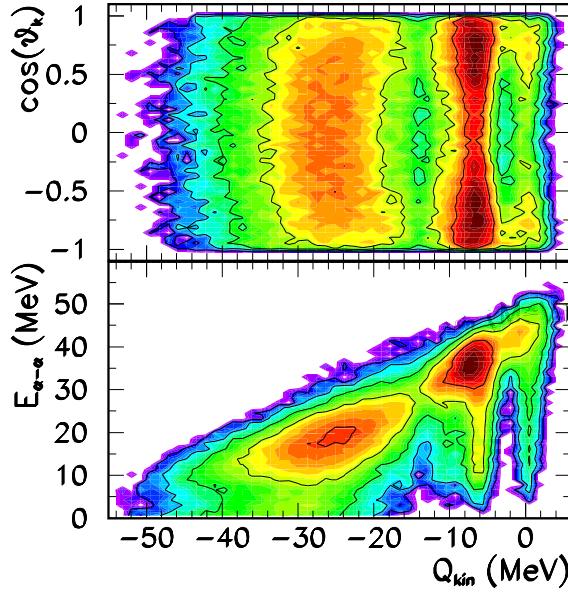


Figure 8. (Color online) Logarithmic contour plot of the correlation between $\cos(\theta_k)$ (upper panel) and the α - α relative energy (lower panel) as a function of Q_{kin} (2) in O- α - α complete events.

To better understand the physical processes leading to the α - α - ^AO channels, we turn to study in greater detail the topology of these three-body coincidence events as revealed by their kinematic correlations.

Dealing with three-body systems, a useful representation can be obtained making use of Jacobi energy-angular correlations, described in detail in [22].

We limit ourselves to the study of the correlations between the two α -particles in the T-system, where the core is the Oxygen. Here, one of the coordinates is the cosinus of the relative angle θ_k of the Oxygen residue momentum \vec{k}_O and the α - α relative momentum $\vec{k}_{\alpha-\alpha}$ [21]: $\cos(\theta_k) = (\vec{k}_O \cdot \vec{k}_{\alpha-\alpha}) / (k_O k_{\alpha-\alpha})$.

The other coordinate is $\epsilon = E_{\alpha-\alpha} / E_T$, i.e. the ratio of the relative energy between the two α 's to the total available energy. In our case, for more dissipative $Q_{<}$ events the undetected neutron prevents the calculation of the normalized relative energy ϵ , but $\cos(\theta_k)$ can still be used.

Figure 8 shows the $\cos(\theta_k)$ (upper panel) and the α - α relative energy (lower panel) distribution as a function of Q_{kin} (1, 2) in O- α - α complete events.

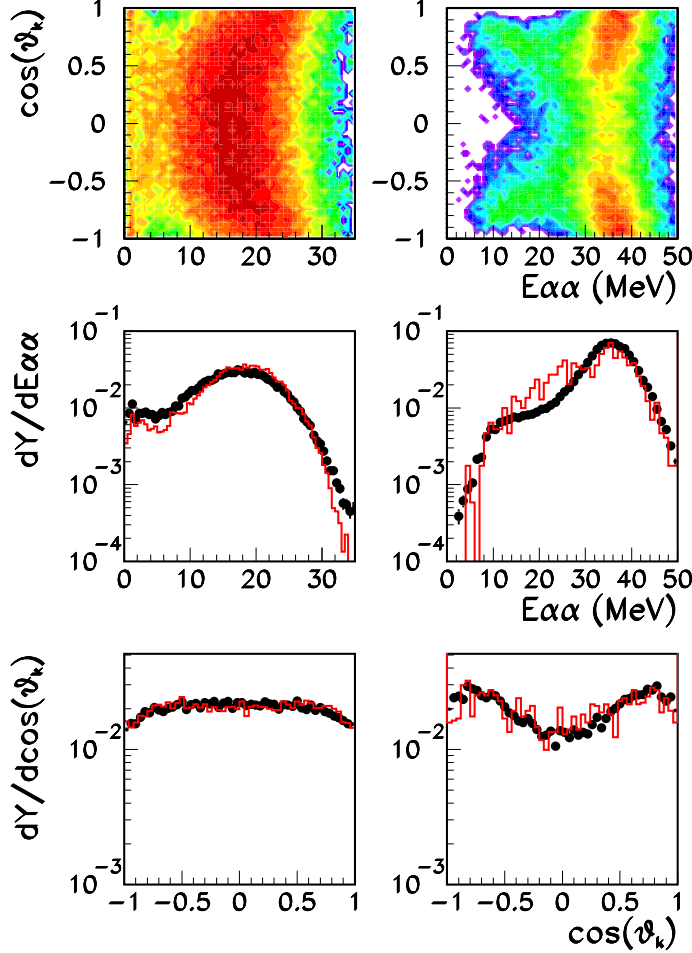


Figure 9. (Color online) Left panels correspond to more dissipative and right panels to less dissipative O- α - α complete events. Upper panels: Logarithmic contour plot of the correlation between $\cos(\theta_k)$ and the α - α relative energy. Middle panels: projections of the α - α relative energy. Lower panels: projections of the angular correlation $\cos(\theta_k)$. Data (symbols) are compared to HFell calculations (lines). All distributions are normalized to the unitary area.

We can recognize that the two dissipation event classes $Q_{<}$ and $Q_{>}$ defined in the previous section correspond to radically different patterns of relative α - α motion. Non-dissipative events are characterized by a relative energy that can overcome 80% of the total available energy, and a back-to-back emission with respect to the oxygen residue. More dissipative events correspond to particles closer in momentum space, consistent with an increased memory loss of the entrance channel. For these events, the $\cos(\theta_k)$ angular distribution is essentially flat.

The energy and angular correlations for the two classes of dissipation are separately

shown in Figure 9, where data are compared to model predictions.

As far as the relative $\alpha - \alpha$ energy is concerned (middle panel) we can recognize two distinct contributions in the $Q_{>}$ distribution. The dominant bump corresponds to the ground state of ^{16}O , while the lower energy shoulder is due to the population of the excited particle bound states, as we have already observed commenting the Q_{kin} distribution (Figure 8). More interesting, two contributions are also visible in the distribution associated with more dissipative events. The small peak at low relative energies suggests that a part of the observed 2- α emission might be associated with a correlated Be state.

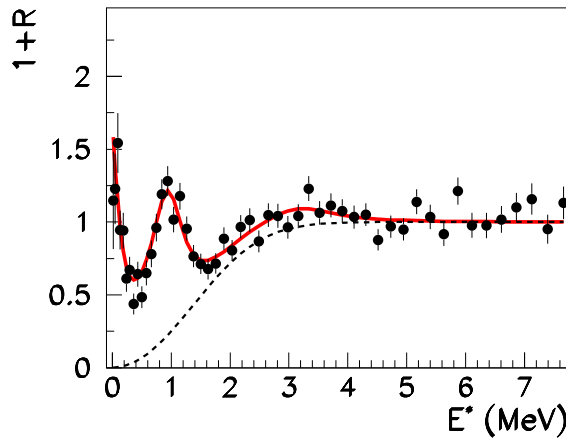


Figure 10. (Color online) Correlation function of the relative $\alpha - \alpha$ energy in the $\alpha - \alpha - ^A\text{O}$ channel (symbols), and corresponding fit (solid line) using the technique of [23]. Dashed line: estimated Coulomb background.

To explore this possibility, we analyzed the $\alpha - \alpha$ correlation function, obtained as the ratio of the measured and uncorrelated distributions. This correlation function, shown in Figure 10, can be very well fitted assuming a convolution of Breit-Wigner distributions corresponding to the different low-lying ^8Be and ^9Be states. For the details about the correlation function technique, see [23]. A clear contribution of ^8Be ground state and first excited state (3.03 MeV) is visible in the figure, as well as the ^9Be ground state at a relative energy of about 1 MeV. The statistical model calculation produces a completely flat correlation function and fails to reproduce these structures. It is important however to point out that events associated with the formation of discrete Be levels do not represent more than 3% of the experimental yield in the more dissipative $^A\text{O}-2\alpha$ channel, and can not be responsible for the global excess in the branching ratio.

Coming to the angular correlation of Figure 9, in the case of a simultaneous three-

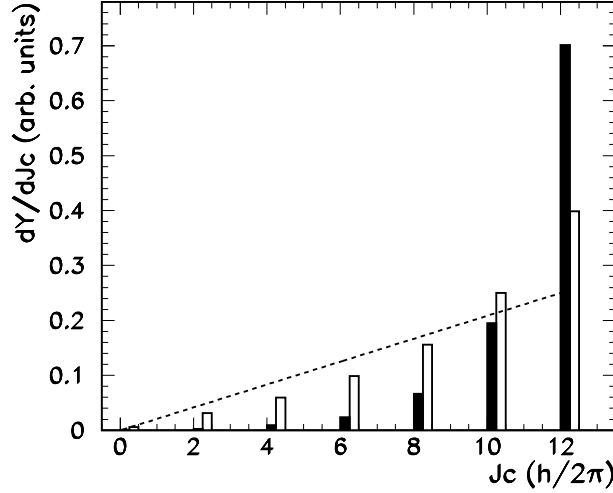


Figure 11. (Color online) Compound angular momentum distribution in the unfiltered HF ℓ calculations associated with different emission channels containing oxygen residues. More dissipative channels are represented by the white histogram, less dissipative by the black histogram. A shift of $0.25 \hbar$ has been applied to the $Q_{<}$ events for a better representation. The distributions are normalized to the unitary area. The dashed line represents the global triangular distribution assumed for the compound.

repulsion [22]. Therefore, the observed flat distribution associated with $Q_{<}$ appears compatible with sequential emission. This is confirmed by the fact that the shape of the distribution is well reproduced by the HF ℓ calculations. The sequential statistical model correctly reproduces also the forward-backward peaked distribution of $Q_{>}$ events. This shape can be understood as due to angular momentum effects. Indeed a high angular momentum of the emitting source introduces a preferential emission direction for the first evaporated particle. The relative momentum vector $\vec{k}_{\alpha-\alpha}$ tends to keep this direction if the second emission is isotropic, which happens if the first particle takes away most of the initially available angular momentum.

This interpretation is confirmed by inspection of Figure 11. This figure displays the compound angular momentum distribution in the unfiltered HF ℓ calculations associated with different emission channels containing Oxygen residues. We can see that the angular momentum distribution is considerably steeper for $^{16}\text{O}-\alpha-\alpha$, that is $Q_{>}$ events, with respect to the global triangular distribution assumed for the compound. More dissipative channels involving neutron emission are associated with a higher thermal excitation energy, and therefore lower rotational energy in order to conserve the total available compound nucleus energy. The reduced angular momentum for this class of events can therefore explain the observed isotropic $\cos(\theta_k)$ distribution. We can conclude

that the Jacobi angular correlations of both dissipation event classes are compatible with sequential decay from an evaporation source. However we recall that the branching ratio towards two- α decay associated with the Oxygen residue shows an important excess in the experiment compared to the $\text{HF}\ell$ calculation for both classes of dissipation. For this reason, we can not interpret the good reproduction of the $\cos(\theta_k)$ distribution by the model as a proof of standard statistical decay in the data.

Concerning the $Q_>$ events, it is important to notice that the kinematical focussing is also compatible with the picture of an incomplete fusion, with two α particles left over from the two α -clustered collision partners. This latter mechanism is indeed the most probable origin of ($^{16}\text{O}-\alpha-\alpha$) events, as we have argued in the previous section. This shows that the interpretation of Jacobi kinematic correlations should be handled with caution.

Concerning the most dissipative ($^4\text{O}-\alpha-\alpha$) events, the strong effect of angular momentum on the $\cos(\theta_k)$ distribution suggests that this observable can be used to explore the effect of the undetected neutron(s) on the $\alpha-\alpha$ kinematical correlations and gather further insight in the physical process at play.

This is shown in Figure 12, where we compare the experimental distribution with the $\text{HF}\ell$ predictions corresponding to different evaporation sequences. The corresponding angular momentum distributions of the initial ^{24}Mg compound are also displayed in bottom panels of the same figure.

When the neutron is the first particle emitted from ^{24}Mg (panel a) and the two α 's correspond to the last two steps of the de-excitation chain, the distribution is single-peaked. Indeed the evaporation sequence corresponds to the lowest average angular momentum for the initial compound (panel d), and moreover the angular momentum available for the first α emission is reduced by the first step of the de-excitation. Conversely, if the two α 's are the first and last emitted particles, with the neutron being emitted in the intermediate step (panel b), the distribution shows two clear peaks. This is consistent with two sequential emissions from a high J source and a low J source, as discussed above. An intermediate situation is observed in panel c), which displays the $\cos(\theta_k)$ distribution obtained when two successive α 's are emitted from the excited ^{24}Mg , and the residual ^{16}O is excited above the neutron separation energy, leading to neutron emission in the last evaporation step. In this case the initial angular distribution is compatible with the one of panel b), but the angular momentum of the ^{20}Ne is not negligible. As a consequence, the second emission leads to a modification of the direction of $\vec{k}_{\alpha-\alpha}$ with respect to the first α emission angle, and a smoothing of the two-peaked distribution.

From Figure 12 we can conclude that the measured distributions are closer to the kinematical configuration expected for the $\alpha-\alpha-n$ sequence. In turn, this implies that the preferential α emission observed in the data can be attributed to the excited state of ^{24}Mg and/or ^{20}Ne .

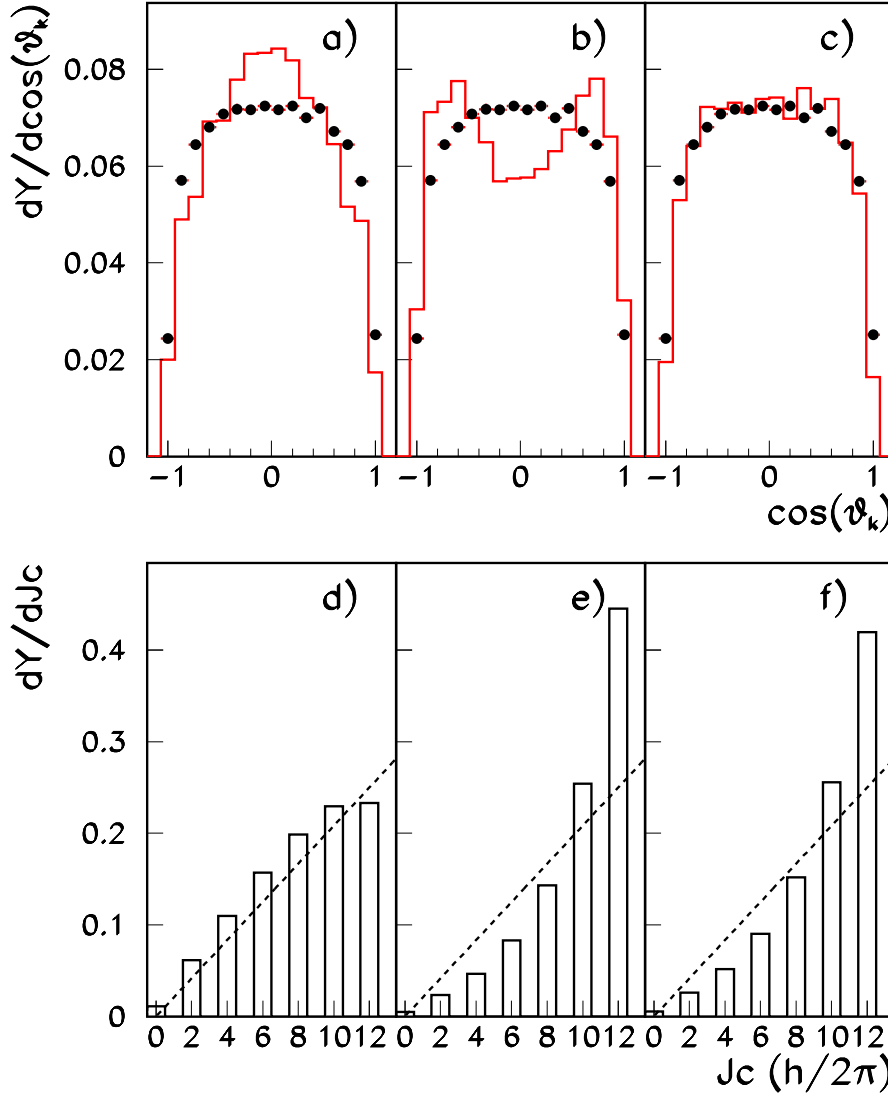


Figure 12. (Color online) Analysis of dissipative $^{15}\text{O}+2\alpha$ complete events. Upper part: the experimental (dots) $\cos(\theta_k)$ distribution is compared to the calculated ones (red lines) according to different emission sequences (see text). Lower part: Compound angular momentum distribution in the unfiltered HF ℓ calculations. The dashed line represents the global triangular distribution assumed for the compound.

Panel a) and d): n is the first emitted particle. Panel b) and e): n is the second emitted particle. Panel c) and f): n is the third emitted particle. All distributions are normalized to unitary area.

3.2. $^A\text{C}-\alpha-\alpha-\alpha$ correlations

In the case of the ($^A\text{C}-3\alpha$) channel, the presence of more than three bodies in the exit

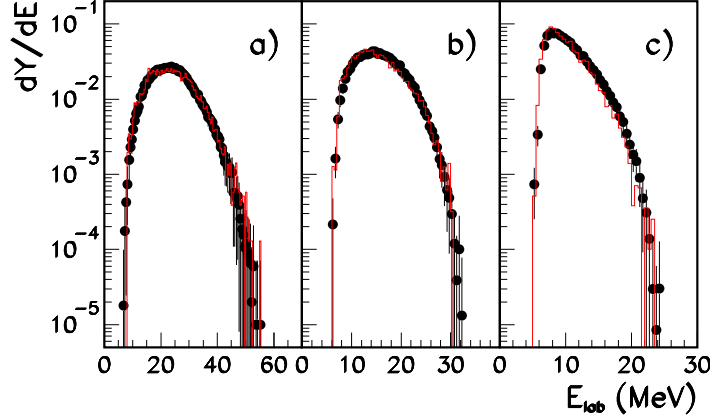


Figure 13. (Color online) Energy spectra of α -particles detected in coincidence with a Carbon residue, ordered in each event according to their laboratory energy as a fast (panel a), medium (panel b) and slow (panel c). Data (symbols) are compared to HF ℓ calculations (lines). All distributions are normalized to the unitary area.

exist that a doorway ^8Be state is populated in the decay associated with this channel, leading again to an effective three body $^{12}\text{C}-\alpha-^8\text{Be}$ problem in the absence of neutron emission, similarly to the Oxygen case. To demonstrate this statement, we have classified the three coincident α -particles in each event as slow, medium and fast according to their laboratory energy [24, 25].

The energy distribution of α -particles is very well reproduced by the model, as shown in Figure 13. This indicates that the kinematics of the decay is well described by a sequential evaporation mechanism.

However, discrepancies between data and model appear in the correlation observables. Indeed, the experimental distributions of $\alpha-\alpha$ relative energy of Figure 14 show clear peaks corresponding to the population of discrete excited states, the highest probability being associated with the two slowest particles of each event. The number of events where two out of the three particles are found with a relative energy below 6 MeV is 40% of the total sample. We can therefore safely argue that a doorway Be state is frequently populated in these events.

The excitation energy distribution of the $^8\text{Be}^*$, reconstructed from the center-of-mass energy of the two α -particles closer in momentum space, is shown in the left part of Figure 15. The contribution of the ground and first excited ^8Be state (3.03 MeV) can be clearly recognized. Model events, analyzed in the same way as the data and shown as a thin blue line in the same panel, show a broad distribution without peaks corresponding to excited states of ^8Be . As discussed in the previous paper [15], in the Hauser-Feshbach formalism, light fragments have a negligible probability to be emitted

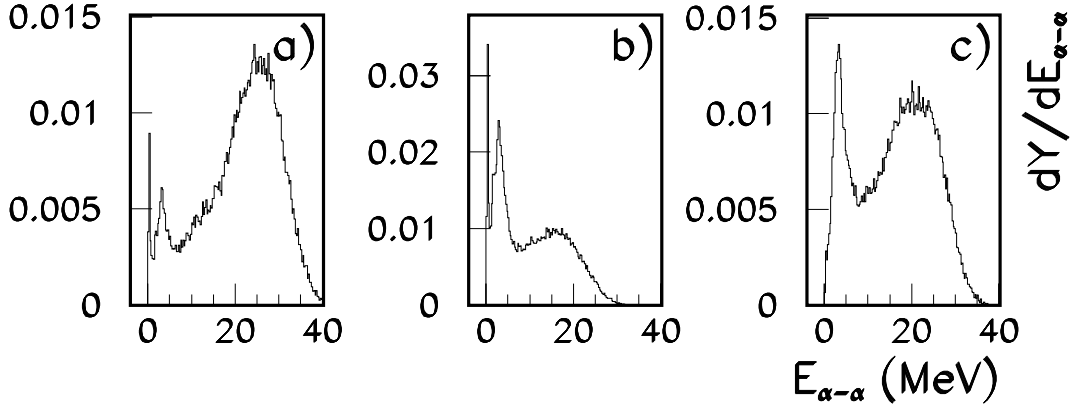


Figure 14. Distribution of relative α - α energy in the $(^{12}\text{C}-3\alpha)$ channel. The three coincident α -particles are ordered in each event according to their laboratory energy as a slow, medium and fast α . Panel a) gives the experimental distribution of relative energy between the fast and the medium, panel b) between the slow and the medium, panel c) between the slow and the fast particle of each event. All distributions are normalized to the unitary area.

and are only obtained as evaporation residues. This discrepancy could be interpreted as the presence of a break-up contribution in the data which is not properly treated by the sequential calculation. Alternatively, it could indicate the existence of correlated alpha structure in the excited even-even nuclei which are explored in the de-excitation chain, as we have already suggested in §2.1.

The contribution of these states is clearly visible in the correlation function drawn in the middle panel, showing the fit through a convolution of Breit-Wigner distributions corresponding to the different low-lying ^8Be states [23].

The Jacobi $\cos(\theta_k)$ distribution in the T -system, obtained replacing the two α -particles with the smallest relative energy by their center-of-mass momentum, is displayed in the right part of Figure 15. The observed kinematic focussing demonstrates that the process is sequential. The existence of an uncorrelated background at ^8Be excitation energies higher than those expected from a population of discrete levels does not change this conclusion. Indeed, the $\cos(\theta_k)$ distribution is not affected by limiting the analysis to $E^* \leq 6$ MeV for the ^8Be spectrum (Figure 15 right panel).

A complementary information on the dynamics of α emission in the Carbon channel can be obtained by using the technique of Dalitz plot [26]. To do this, one has to build the Dalitz coordinates: $x_D = \sqrt{3}/2(E_{rel_{23}} - E_{rel_{12}})$ and $y_D = (2E_{rel_{13}} - E_{rel_{23}} - E_{rel_{12}})/2$ where $E_{rel_{ij}}$ is the relative energy of the i -th and j -

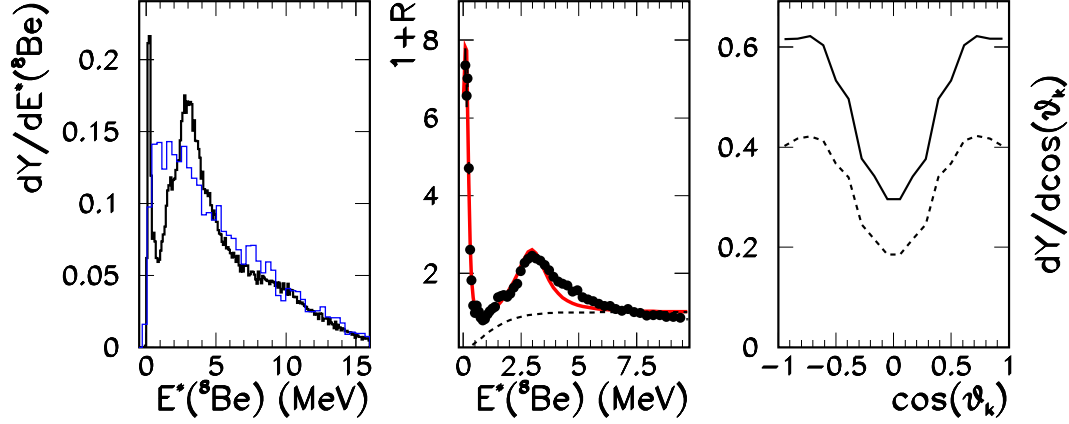


Figure 15. (Color online) Left panel: Excitation energy distribution of the reconstructed $^8\text{Be}^*$ in the $^4\text{C}-3\alpha$ channel. In each event, the two α -particles with the smallest relative energy are selected. The thin blue line represents HF ℓ predictions. Middle panel: Correlation function of the $^8\text{Be}^*$ excitation energy (symbols), and corresponding fit (solid line) using the technique of [23]. Dashed line: estimated Coulomb background. Right panel: Jacobi $\cos(\theta_k)$ distribution in the T -system obtained replacing the the two α -particles with the smallest relative energy by their center-of-mass momentum. Full line: all events. Dashed line: analysis limited to a reconstructed ^8Be excitation energy $E^* \leq 6$ MeV. All distributions are normalized to the number of events.

th particles. The Dalitz plots for the $3 - \alpha$ coincidences are shown in Figure 16, with

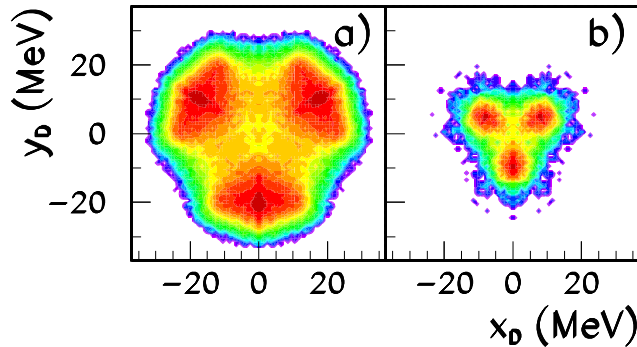


Figure 16. (Color online) α Dalitz plot in the $^4\text{C}-3\alpha$ channel for low dissipation (a) and high dissipation (b).

different dissipation cuts. Independently of the dissipation, the Dalitz plot clearly shows three bumps indicating a sequential process [26]. The dissipation is obviously correlated with the excitation energy. The excitation energy considered in the present case is much higher than the $3-\alpha$ Hoyle state of ^{12}C , and discrete Carbon states decaying into three α -particles are not populated in the experimental sample, due to the high beam energy and the selection of central events.

The information given by the correlation studies reported in Figures 15 and 16 consistently indicates a sequential evaporation of α -particles from an excited ^{24}Mg leaving a Carbon residue, and tends to exclude the excitation of a binary quasi-molecular $(^{12}\text{C}+^{12}\text{C})^*$ state. Similarly to the Oxygen case, the main deviation from a standard statistical behaviour concerns the branching ratio of the channel. This again indicates a preferential α emission from the compound ^{24}Mg and/or its daughter nucleus ^{20}Ne . In the Carbon case, a non-negligible (40%) fraction of the events corresponds to a correlated alpha emission as a doorway ^8Be . This feature is also not reproduced by the statistical model.

3.3. $6-\alpha$ coincidences

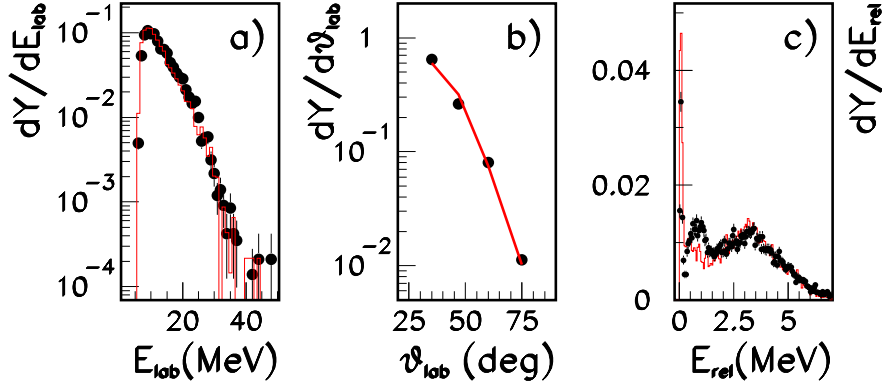


Figure 17. (Color online) Analysis of $6-\alpha$ coincidences (symbols), compared to HF predictions (lines). Panel a): α energy spectrum. Panel b): α angular distribution. Panel c): $\alpha-\alpha$ relative energy distribution. All distributions are normalized to unitary area.

Finally, we turn to examine events where the whole available mass and charge is found as α -particles. The branching ratio of this channel is well reproduced by the statistical model, as we have already observed in Figure 1. It is however interesting to check if the kinematical properties of the observed events are compatible with a

The ensemble of the different α observables are presented in Figure 17, in comparison with the statistical model predictions. We can see that the model successfully reproduces the kinematic characteristics of these events. In panel c) we can recognize the ground state and the first excited state of ^8Be (3.03 MeV), which are well reproduced by the model. The experimental distribution of the $\alpha - \alpha$ relative energy shows an extra-peak at about 1 MeV, not seen in the model. It corresponds to the ground state of ^9Be and it is due to a $^3\text{He}-\alpha$ contamination of $Z = 2$ particles at the limit of the mass identification threshold, as already observed in Figure 5. The contribution of this contamination has been evaluated to be about 7%. If we ignore this spurious contribution, we can estimate that the events showing a ^8Be correlation with an excitation energy below 6 MeV are 90% of the $6 - \alpha$ -particles sample, in agreement with the statistical model. The presence of these Beryllium correlations shows that the six- α emission is fully compatible with a sequence of binary decays, with the last evaporation step leaving an unstable ^8Be residue [27].

4. Conclusions

The $^{12}\text{C}(^{12}\text{C}, X)$ reaction has been studied at 95 MeV beam energy with the GARFIELD+RCO experimental setup at LNL-INFN. Events completely detected in charge ($Z_{tot} = 12$) have been selected and compared to Hauser Feshbach statistical model calculations performed with the code HF ℓ .

Some clear deviations from a statistical behaviour in the decay have been found. These deviations concern an anomalously high branching ratio towards multiple (two or three) α emission. Conversely, the probability of a complete vaporisation into six α -particles is well reproduced. This latter channel is shown to be compatible with a standard statistical sequential emission, leading to a final unstable ^8Be evaporation residue.

Two different phenomena can explain the extra yield in the 2 and 3 α -particle exit channels. First, an extra experimental cross section for the three-body less dissipative $^{16}\text{O}-\alpha - \alpha$ decay channel has been attributed to the contamination of direct reactions. This reaction mechanism mixing is not the unique source of discrepancy with the HF ℓ predictions.

Despite these events have been excluded and all the kinematic characteristics were reproduced, the branching ratios of the multiple α -decay channels were found to be still largely underestimated by the calculation.

A detailed analysis of the multiple α -particle correlations in these channels indicates a sequential process with a clear hierarchy in the emission sequence. The highest probability is associated with the first chance emission of an α -particle from a highly excited ^{24}Mg compound, leaving the daughter ^{20}Ne nucleus still well above its particle emission threshold. Then, the excited ^{20}Ne preferentially emits another α -particle, leaving an Oxygen final evaporation residue, or alternatively an excited ^8Be nucleus in coincidence with a Carbon residue. Neutron emission was not directly

measured, but it was attributed to the last emission step, according to kinematical correlations. As a general conclusion, the persistence of cluster structures for ^{24}Mg and/or its daughter nucleus ^{20}Ne , at excitation energies well above the energy threshold for full disintegration into α -particles, can be inferred.

Acknowledgments

The authors thank the crew of the XTU TANDEM acceleration system at LNL.

This work was partially supported by the European Funds for Large Scale Facilities - Seventh Framework Program - ENSAR 262010 and by grants of Italian Ministry of Education, University and Research under contract PRIN 2010-2011.

References

- [1] Ikeda K, Tagikawa N. and Horiuchi H 1968 *Prog. Theor. Phys. Suppl.* **E68** 464; Horiuchi H, Ikeda K and Kato K 2012 *Prog. Theor. Phys. Suppl.* **192** 1.
- [2] Freer M 2007 *Rep. on Prog. in Phys.* **70** 2149.
- [3] Wiringa R B, Pieper S C, Carlson J and Pandharipande V R 2000 *Phys. Rev. C* **62** 014001; Kanada-Enyo Y and Horiuchi H 2001 *Prog. Theor. Phys. Suppl.* **142** 205; Neff T and Feldmeier H 2004 *Nucl. Phys.* **A738** 357.
- [4] Takemoto H *et al* 2004 *Phys. Rev. C* **69** 035802.
- [5] Maruhn J A, Kimura M, Schramm S, Reinhard P-G, Horiuchi H and Tohsaki A 2006 *Phys. Rev. C* **74** 044311; Reinhard P-G, Maruhn J A, Umar A S and Oberacker V E 2011 *Phys. Rev. C* **83** 034312.
- [6] Girod M 2013 contribution to the *ESNT workshop on localization and clustering in atomic nuclei* <http://esnt.cea.fr>
- [7] Ebran J P, Khan E, Niksic T and Vretenar D 2012 *Nature* **487** 341.
- [8] Costanzo E *et al* 1991 *Phys. Rev. C* **44** 111; Grenier F *et al* 2008 *Nucl. Phys.* **A811** 233; Raduta Ad R *et al* 2011 *Phys. Lett. B* **705** 65; Kokalova Tz, Itagaki N, von Oertzen W and Wheldon C 2006 *Phys. Rev. Lett.* **96** 192502; von Oertzen W *et al* *Eur. Phys. Journ. A* **36** 279; Di Pietro A *et al* 2012 *Journal of Physics: Conference Series* **366** 012013; Vardaci E *et al* 2013 *Journal of Physics: Conference Series* **436** 012054 and references quoted therein.
- [9] Cosman E R *et al* 1975 *Phys. Rev. Lett.* **35** 265; Bremner C A *et al* 2002 *Phys. Rev. C* **66** 034605; Cormier T M, Jachcinski C M, Berkowitz G M, Braun-Munzinger P, Cormier P M, Gai M, Harris J W, Barrette J and Wegner H E 1978 *Phys. Rev. Lett.* **40** 924; Morsad A, Haas F, Beck C and Freeman R M 1991 *Z. Phys. A* **338** 61.
- [10] Wuosmaa A H *et al* 1992 *Phys. Rev. Lett.* **68** 1295; Aliotta M *et al* 1995 *Z. Phys. A* **353** 43; Le Marechal R A *et al* 1997 *Phys. Rev. C* **55** 1881.
- [11] Takashina M *et al* 2004 *Nucl. Phys.* **A738** 352.
- [12] Baiocco G *et al* 2013 *Phys. Rev. C* **87** 054614.
- [13] Baiocco G 2012 *PhD Thesis, Università di Bologna and Université de Caen Basse-Normandie* <http://amsdottorato.cib.unibo.it/4295/>.
- [14] Tarasov O. B. and Bazin D 2003 *Nucl. Instrum. Methods B* **204** 174.
- [15] Morelli L *et al* first paper of this series.
- [16] M. Bruno *et al* 2013 *Eur. Phys. Journ. A* **49** 128.
- [17] Morelli L *et al* arXiv:nucl-ex/1309.0323 Contr. to *25th International Nuclear Physics Conference (INPC 2013) Firenze, Italy*.
- [18] Rivet M F *et al* 1996 *Phys. Lett. B* **388** 219.
- [19] Hagel K *et al* 2012 *Phys. Rev. Lett.* **108** 062702.
- [20] Matsumura H and Suzuki Y 2004 *Nucl. Phys. A* **739** 238; Yamada T and Schuck P 2004 *Phys. Rev. C* **69** 024309.

- [21] Ohlsen G G 1965 *Nucl. Instrum. Methods* **37** 240.
- [22] Pfützner M, Karny M, Grigorenko L V and Riisager K 2012 *Rev. Mod. Phys.* **84** 567; Grigorenko L V *et al* 2009 *Phys. Rev. C* **80**034602; Egorova I A *et al* 2012 *Phys. Rev. Lett.* **109** 202502; Charity R *et al* 2011 *Phys. Rev. C* **84** 014320.
- [23] D'Agostino M *et al* 2011 *Nucl. Phys.* **A861** 47; D'Agostino M *et al* 2012 *Nucl. Phys.* **A875** 139.
- [24] Freer M 1994 *Phys. Rev. C* **49** R1751.
- [25] Rana T K *et al* 2010 *Proceedings of the DAE Symp. on Nucl. Phys.* **55** 230.
- [26] Dalitz R H 1953 *Phil. Mag.* **44** 1068.
- [27] Di Pietro A *et al* 1999 *Phys. Rev. C* **59** 1185.